Continental Shelf Research 186 (2019) 13–20

Contents lists available at ScienceDirect

Continental Shelf Research

journal homepage: www.elsevier.com/locate/csr

Research Note

Temporal changes in the response of the nodal modulation of the M_2 tide in the Gulf of Maine

Haidong Pan[a,b,**], Quanxin Zheng[a,b], Xianqing Lv[a,b,*]

[a] Key Laboratory of Physical Oceanography, Ocean University of China, Qingdao, 266003, China
[b] Qingdao National Laboratory for Marine Science and Technology, Qingdao, 266100, China

ARTICLE INFO

Keywords:
Enhanced harmonic analysis
Tides
Nodal cycle
Gulf of Maine

ABSTRACT

Accurate estimation of the changes of tides is important for sea level prediction and fundamental for local coastal planning. Here we use a novel method, enhanced harmonic analysis (EHA), to extract temporal changes in the response of the nodal modulation of the M_2 tide in the Gulf of Maine. The results show that the temporal variations of nodal amplitudes at four stations in the Gulf of Maine are similar from 1970s to 2013. They all increase in the 1970s to peak values in the 1985s and in the 2000s they decrease to minimum values. The North Atlantic Oscillation (NAO), which is one of the major climate modes in the North Atlantic Ocean, may be responsible for temporal changes in the response of the nodal modulation of the M_2 tide from 1970s to 2013. Also, the results obtained by the new method indicate that the traditional method of harmonic analysis slightly underestimates the trend of M_2 amplitude in the Gulf of Maine.

1. Introduction

All lunar constituents are modulated by the 18.61 year nodal cycle induced by the precession of the lunar ascending node (Feng et al., 2015). In case of a linear response of the ocean to tidal forcing, the amplitude of the M_2 nodal cycle is 3.73% of the tidal amplitude, the amplitude of the K_1 nodal cycle is 11.5% of the tidal amplitude and the amplitude of the O_1 nodal cycle is 18.7% of the tidal amplitude which are implicitly indicated by the tidal potential (Müller, 2011). However, due to the effect of bottom friction on the tidal signal, the observed nodal modulation of M_2 amplitude has been found to be less than that predicted by the equilibrium theory in several regions around the world (Feng et al., 2015). For example, Ku et al. (1985) found that nodal modulation of M_2 amplitude in the Gulf of Maine is reduced from 3.73% to 2.4% by the effects of friction and resonance.

Traditionally, the harmonic parameters of the 18.61 year cycle as well as the long-term trends are estimated by a least squares model (Ku et al., 1985; Ray, 2006, 2009; Jay, 2009; Feng et al., 2015). The expression of the joint estimation is described as:

$$P(t) = A_0 + A_1 t + a\cos\left(\frac{2\pi}{18.61}t\right) + b\sin\left(\frac{2\pi}{18.61}t\right) \quad (1)$$

where $P(t)$ is the estimated value of tidal properties (amplitude or phase) at time t (in the unit of year). A_0 is a constant. A_1 is the linear trend. a and b are the amplitudes of the cosine and sine functions of the nodal cycle. After fitting Eq. (1), amplitude (H_N) and phase (G_N) of the nodal cycle can be obtained as:

$$H_N = \sqrt{a^2 + b^2}$$
$$G_N = \arctan(b/a) \quad (2)$$

Ray (2006) first reported that the large positive trend in the M_2 amplitude at four stations in the Gulf of Maine (Fig. 1), evident since 1890, abruptly stopped in the early 1980s. Fig. 2 shows the yearly estimated M_2 amplitudes at Eastport. As we can see clearly from the red box in Fig. 2, the M_2 amplitudes abruptly dropped in the early 1980s. In Ray's study, the amplitude and phase of nodal cycle are assumed as constants and estimated by Eq. (1) and Eq. (2). In this paper, we hypothesize that the response of the nodal modulation of the M_2 tide in the Gulf of Maine has experienced long time changes (i.e., H_N and G_N are time-varying) due to an abrupt shift in the 1980s; this is also the likely reason for changes in the long term trend of M_2.

The purpose of this report is twofold: 1) to introduce a new methodology that is suitable to extract modifications in the local nodal cycle response and 2) to evaluate the effect of a changing nodal response on the estimation of long-term trend of M_2 amplitude in the Gulf of Maine. The paper is organized as follows. Study site、data and methodology are described in section 2. Section 3 shows the results and the

* Corresponding author. Key Laboratory of Physical Oceanography, Ocean University of China, Qingdao, 266003, China.
** Corresponding author. Qingdao National Laboratory for Marine Science and Technology, Qingdao, 266100, China.
E-mail addresses: panhaidong_phd@qq.com (H. Pan), xqinglv@ouc.edu.cn (X. Lv).

https://doi.org/10.1016/j.csr.2019.07.007
Received 24 March 2019; Received in revised form 4 July 2019; Accepted 8 July 2019
Available online 13 July 2019

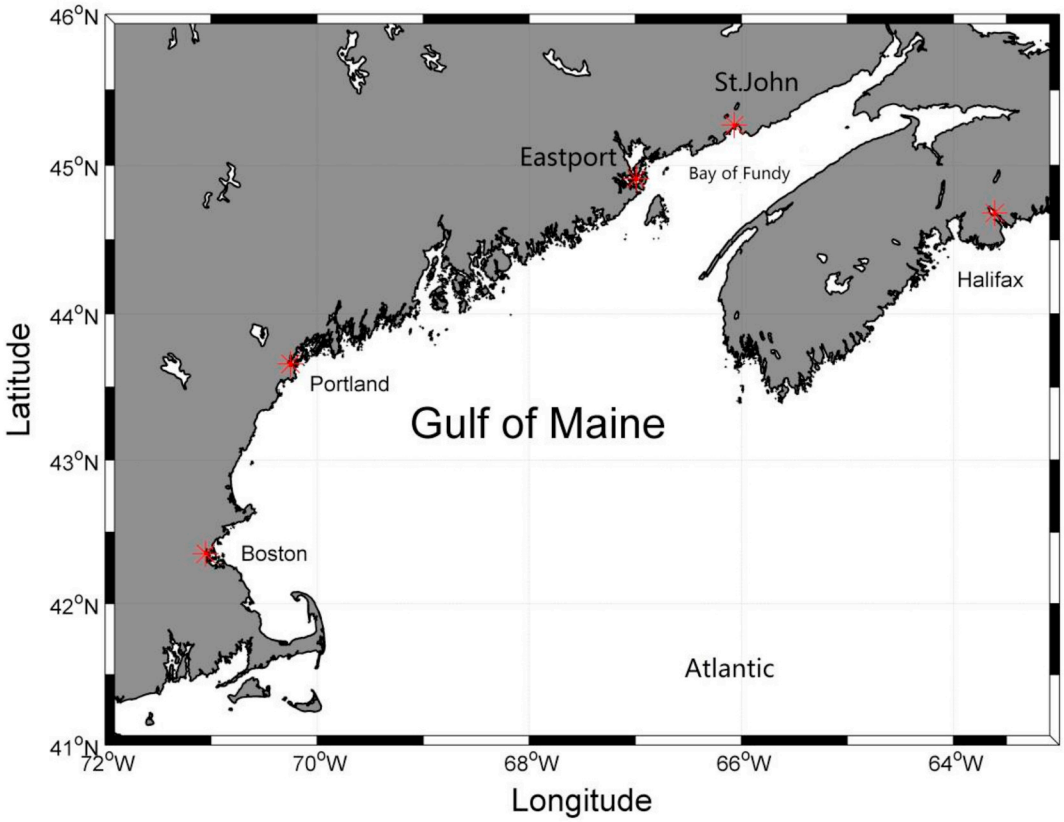

Fig. 1. Map of the Gulf of Maine and the location of tide gagues.

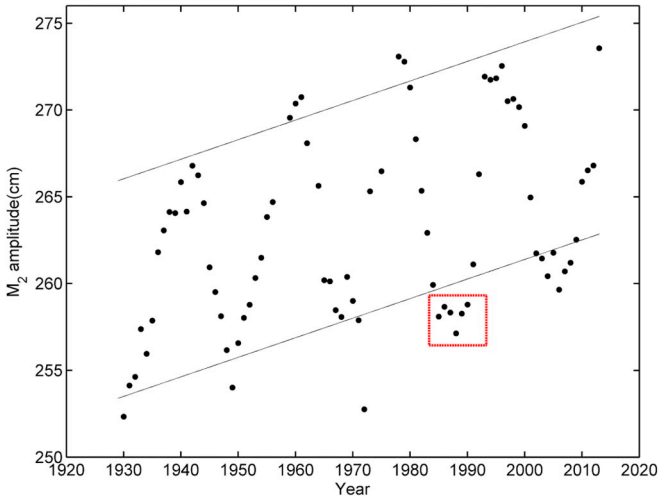

Fig. 2. Yearly estimates of the M2 amplitudes at Eastport. As we can see clearly from the red box, the M2 amplitudes abruptly dropped in the early 1980s. (For interpretation of the references to colour in this figure legend, the reader is referred to the Web version of this article.)

performance of our proposed method, followed by the conclusions in Section 4.

2. Study site data and methodology

2.1. Study site

The Gulf of Maine has one of the world's most dynamic environments (Ku et al., 1985; Godin, 1992). This semi-enclosed continental shelf sea is nourished by cold ocean waters and characterized by a complex geomorphology made up of deep basins and shallow banks (Wang et al., 2017). Tides in the Gulf of Maine are the highest in the world due to resonance of the semidiurnal tides (Ku et al., 1985). The large tidal range makes the Gulf of Maine a desirable location for tidal power plants. Pelling and Green (2013) investigated the response of the Bay of Fundy and Gulf of Maine to large-scale tidal power plants using a numerical tidal model. Katavouta et al. (2016) investigated the seasonal and tidal variability of the Gulf of Maine and Scotian shelf, and their dynamical interaction using a high-resolution circulation model.

Tides in the Gulf of Maine show a significantly higher trend than other regions (Godin, 1992, 1995). The rapidly changing tides increase the risk of flooding in this system. Greenberg et al. (2012) indicated that even in the absence of global warming, high water in the Gulf of Maine is likely to rise on the order of 0.3 m over the next century due to the existing trends in tidal range and mean sea level. Ray and Foster (2016) analyzed observed water levels at Boston which sits in the lower Gulf of Maine and indicated that tidal flooding will become more frequent in subsequent years.

2.2. Data

Hourly water level records from St. John, Eastport, Portland, and Boston in the Gulf of Maine (Fig. 1) were analyzed. Additional water level observations at Halifax, which is directly open to the Atlantic Ocean, were also analyzed. Tide data in the Gulf of Maine were provided by the University of Hawaii Sea Level Center (https://uhslc.soest.hawaii.edu/), and observations from Halifax were provided by Fisheries and Oceans Canada (http://www.isdm-gdsi.gc.ca/isdm-gdsi/twl-mne/inventory-inventaire/interval-intervalle-eng.asp?user=isdm-gdsi&region=ATL&tst=1&no=65&ref=maps-cartes).

Hourly water level records are divided into yearly windows with each window subjected to independent tidal analysis using T_TIDE (Pawlowicz et al., 2002). However, if the missing data points in one

Table 1
Information of tide gauges in the Gulf of Maine. AL = Abandoned Length; TL = Total Length.

Station	Timespan	Total Length (year)	Abandoned Length (year)	AL/TL
St.John	1906–2013	108	20	18.52%
Eastport	1929–2013	85	7	8.24%
Portland	1910–2013	104	4	3.85%
Boston	1921–2013	93	2	2.15%
Halifax	1920–2013	94	0	0%

year exceed 30%, this yearly window will be excluded. As shown in Table 1, St.John has the longest water level records (108 years), but it also has the longest abandoned records (20 years).

2.3. Methodology

Jin et al. (2018) proposed the EHA and applied it to determine the temporal variations for the four principal constituents of internal tides in the South China Sea. Pan et al. (2018b) developed S_TIDE Matlab toolbox to realize EHA and used it to explore the tidal-fluvial interaction in the Columbia River Estuary. Here, we use EHA to calculate time-varying amplitude and phase of the local nodal cycle response. Thus, Eq. (1) is modified as:

$$P(t) = A_0 + A_1 t + a(t)\cos\left(\frac{2\pi}{18.61}t\right) + b(t)\sin\left(\frac{2\pi}{18.61}t\right) \tag{3}$$

Eq. (3) is solved with the independent point (IP) scheme (Guo et al., 2017; Lu and Zhang, 2006; Pan et al., 2017). The main idea of the IP scheme is expressed in the following procedures. The time-varying harmonic parameters of the 18.61 year cycle (denoted as $a(t)$, and $b(t)$) at IPs, which are uniformly distributed in the time domain, are selected as independent parameters (denoted as a_i and b_i), and those at other points are obtained by interpolation between the IPs (Pan et al., 2018b). Thus, $a(t)$, and $b(t)$ can be expressed by linear combinations of a_i and b_i which are

$$\begin{aligned} a(t) &= \textstyle\sum_{i=1}^{M} f_{t,i}\, a_i \\ b(t) &= \textstyle\sum_{i=1}^{M} f_{t,i}\, b_i \end{aligned} \tag{4}$$

where $f_{t,i}$ is the interpolation weight for the i-th IP at time t, which depends on the interpolation method. M is the IP number for harmonic parameters. a_i and b_i are unknown at present, but through the IP scheme, the time-varying $a(t)$ and $b(t)$ can be obtained by interpolating a_i and b_i. Therefore, the procedures to solve a_i and b_i are pivotal in EHA and expressed in the following.

Combination of Eq. (3) and Eq. (4) yields Eq. (5)

$$P(t) = A_0 + A_1 t + \sum_{i=1}^{M} f_{t,i}\, a_i \cos\left(\frac{2\pi}{18.61}t\right) + \sum_{i=1}^{M} f_{t,i}\, b_i \sin\left(\frac{2\pi}{18.61}t\right) \tag{5}$$

In this paper, the cubic spline interpolation is implemented in the EHA due to its stable, convergent and smooth characteristics (Huang et al., 1998; Pan et al., 2018b; Pan and Lv, 2019; Zong et al., 2018). Refer to Appendix B in Pan et al. (2018b) for the details of the computation of cubic spline interpolation weights.

With measurements during N years, we can obtain the following equation set:

$$\begin{cases} P(t_1) = A_0 + A_1 t_1 + \sum_{i=1}^{M} f_{t_1,i}\, a_i \cos\left(\frac{2\pi}{18.61}t_1\right) + \sum_{i=1}^{M} f_{t_1,i}\, b_i \sin\left(\frac{2\pi}{18.61}t_1\right) \\ P(t_2) = A_0 + A_1 t_2 + \sum_{i=1}^{M} f_{t_2,i}\, a_i \cos\left(\frac{2\pi}{18.61}t_2\right) + \sum_{i=1}^{M} f_{t_2,i}\, b_i \sin\left(\frac{2\pi}{18.61}t_2\right) \\ \cdots \\ P(t_N) = A_0 + A_1 t_N + \sum_{i=1}^{M} f_{t_N,i}\, a_i \cos\left(\frac{2\pi}{18.61}t_N\right) + \sum_{i=1}^{M} f_{t_N,i}\, b_i \sin\left(\frac{2\pi}{18.61}t_N\right) \end{cases} \tag{6}$$

For convenience, Eq. (6) can be written in matrix form as $\mathbf{P} = \mathbf{B}\mathbf{y}$, where $\mathbf{P}$ is the vector of estimated value of tidal properties (amplitude or phase), $\mathbf{B}$ is the matrix which consists of known interpolation weights, and $\mathbf{y}$ is the unknown parameter vector which comprises a_i and b_i:

$$P = [P(t_1)\ \ P(t_2)\ \ \ldots\ \ P(t_N)]^T \quad y = [A_0\ \ A_1\ \ a_1\ \ \ldots\ \ a_M\ \ b_1\ \ \ldots\ \ b_M]^T$$

$$B = \begin{bmatrix} 1 & t_1 & f_{t_1,1}\cos(\sigma t_1) & \ldots & f_{t_1,M}\cos(\sigma t_1) & f_{t_1,1}\sin(\sigma t_1) & \ldots & f_{t_1,M}\sin(\sigma t_1) \\ 1 & t_2 & f_{t_2,1}\cos(\sigma t_2) & \ldots & f_{t_2,M}\cos(\sigma t_2) & f_{t_2,1}\sin(\sigma t_2) & \ldots & f_{t_2,M}\sin(\sigma t_2) \\ \ldots & \ldots & \ldots & & \ldots & \ldots & & \ldots \\ 1 & t_N & f_{t_N,1}\cos(\sigma t_N) & \ldots & f_{t_N,M}\cos(\sigma t_N) & f_{t_N,1}\sin(\sigma t_N) & \ldots & f_{t_N,M}\sin(\sigma t_N) \end{bmatrix}$$

where

$$\sigma = \frac{2\pi}{18.61} \tag{7}$$

By the method of least squares, the best estimate of $\mathbf{y}$ is given by

$$y = B^{-1}P \tag{8}$$

At last, the changing $a(t)$ and $b(t)$ can be obtained by interpolating a_i and b_i (Eq. (4)). The selection of number of IPs is discussed using sensitivity experiments in the next section.

3. Results and discussions

3.1. Sensitivity experiments

We performed a series of sensitivity experiments, where the number of IPs for the nodal cycle at Portland increased gradually from 3 to 12. As the IP number increases, the hindcasts obtained by EHA are more close to observed M_2 amplitudes (see black box in Fig. 3). It should be noted that 0 IP represents that the amplitude and phase are constant, i.e., using Eq. (1). Table 2 also indicates that when the IP number increases, the root-mean-square error (RMSE) decreases. However, when using too many IPs, the signal-to-noise ratio (SNR) for trend is very low. For example, when using 12 IPs, SNR is only 1.51, which is very low compared to those obtained by other IPs. SNR is important because it represents the reliability of the trend. Due to the low SNR, the trend obtained by 12 IPs may be incorrect. Fig. 4 displays the nodal amplitudes obtained by different numbers of IPs. As the IP number increases, the nodal amplitudes obtained by EHA show more oscillations. However, the nodal amplitudes obtained by 12 IPs seem unrealistic and much bigger than those obtained by other IPs. These exaggerated oscillations induced by overfitting influence the calculation of the trend. As also reported by Pan et al. (2018b), too many IPs in EHA may induce unrealistic results. Therefore, we must choose suitable IP number for the nodal cycle which can produce a relatively low RMSE and a

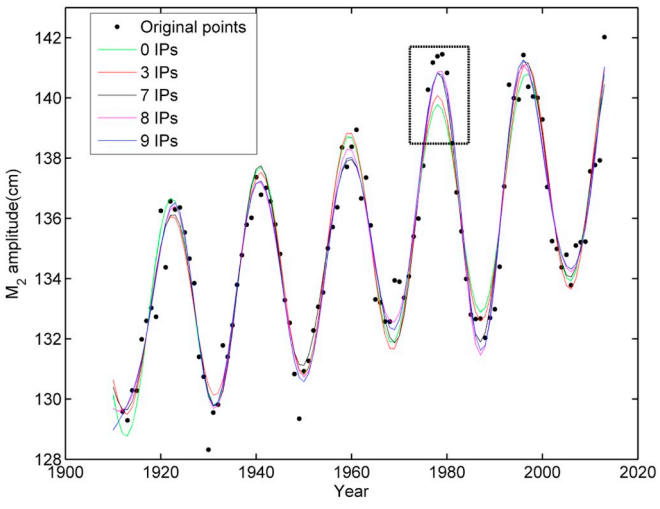

Fig. 3. The hindcasts obtained by EHA with different numbers of IPs (Portland).

Table 2
The results of EHA at Portland. RMSE = root-mean-square error; SNR = signal-to-noise ratio.

IP number	Trend (cm/century)	95% confidence intervals of trend	SNR	RMSE (cm)
0	5.5395	0.5927	9.3457	0.8684
3	5.6396	0.5984	9.4242	0.8302
4	5.5781	0.6243	8.9352	0.8192
5	5.6202	0.5998	9.3704	0.7722
6	5.6819	0.6402	8.8752	0.7779
7	5.7539	0.6458	8.9094	0.7534
8	6.0942	0.6479	9.4058	0.6971
9	6.3994	0.7239	8.8397	0.6945
10	6.6234	0.9333	7.0970	0.6669
11	6.9558	1.5472	4.4959	0.6563
12	3.7145	2.4523	1.5147	0.6061

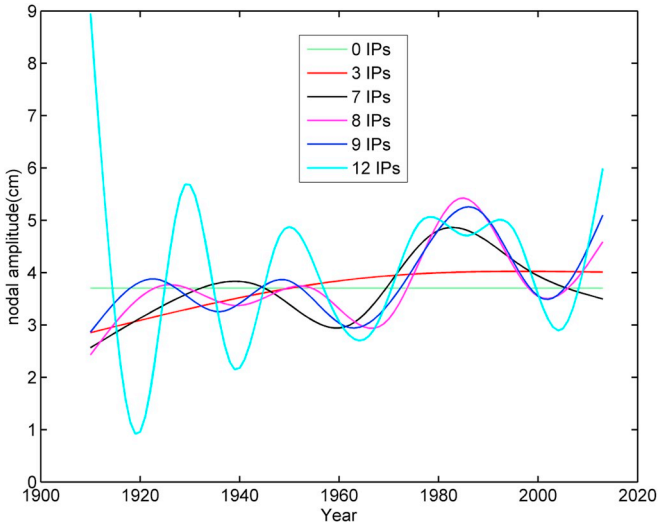

Fig. 4. The nodal amplitudes obtained by EHA with different numbers of IPs (Portland).

relatively high SNR. Here, 9 IPs are suitable for Portland according to Table 2.

We also conduct sensitivity experiments for other stations, the results are displayed in Fig. A1 and Tables A1–A4 in Appendix A. Based on these sensitivity experiments, we select optimal IP number for these stations (see Table 3). It should be noted that St. John has the lowest SNR for trend compared to other four stations (Table 3), which may be caused by the large gap (see Table 1) in water level records.

3.2. Long-term trend of M_2 amplitude in the Gulf of Maine

As displayed in Table 3, traditional least-squares estimate of trends of M_2 amplitude (using Eq. (1)) are: 5.54 cm/century (St. John); 7.59 cm/century (Eastport); 5.54 cm/century (Portland); 2.55 cm/century (Boston); −1.53 cm/century (Halifax). Trends of M_2 amplitude

Table 3
Optimal IPs determined by sensitivity experiments.

Station	Optimal IP number	Trend (classic method)	95% confidence intervals	Trend (EHA)	95% confidence intervals
St.John	10	5.5398	1.8933	3.3144	2.3087
Eastport	7	7.5854	1.6713	7.8151	2.0911
Portland	9	5.5395	0.5927	6.3994	0.7239
Boston	8	2.5544	0.6345	2.9075	0.7715
Halifax	8	−1.5318	0.3738	−2.0342	0.4312

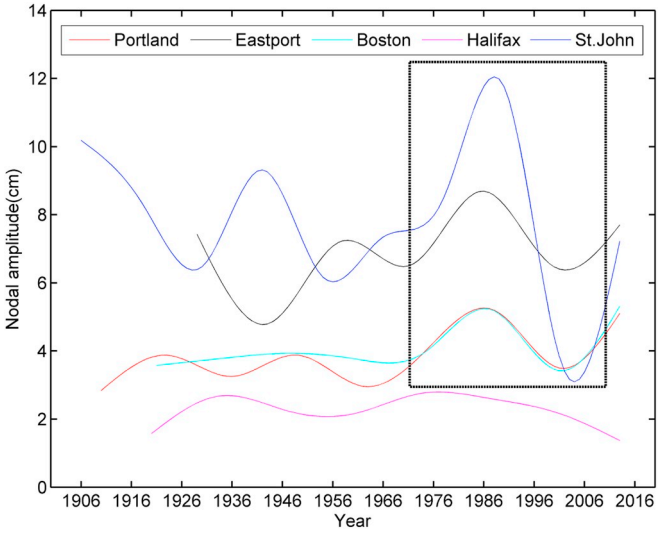

Fig. 5. The nodal amplitudes obtained by EHA at five stations (corresponding IP numbers are displayed in Table 3).

obtained by EHA (using Eq. (3)) are: 3.31 cm/century (St.John); 7.82cm/century (Eastport); 6.40 cm/century (Portland); 2.91 cm/century (Boston); −2.03 cm/century (Halifax).

It seems that the traditional method of harmonic analysis slightly underestimates the trend at Eastport, Portland, Boston and Halifax but obviously overestimates the trend at St. John. Since the trend of St. John has the lowest SNR (less than 2), we are inclined to think that the traditional method of harmonic analysis slightly underestimates the trend of M_2 amplitude in the Gulf of Maine. Also, both methods indicate that long-term trend of M_2 amplitude at Eastport station is significantly larger than other stations in this region.

3.3. Possible causes of temporal changes in the response of nodal modulation of the M_2 tide

The nodal amplitudes of M_2 tides at five stations are shown in Fig. 5. It is not yet clear what the reasons behind the irregular variations in the nodal response. There is no coherence between station results before 1970, even though one station goes back to the 1906. However, as displayed in the black box in Fig. 5, temporal variations of the nodal amplitudes at four stations are similar from 1970s to 2013. They all increase in the 1970s to peak values in the 1985s and in the 2000s they decrease to minimum values. Why did the coherent fluctuations suddenly start in the 1970s? We think that this phenomenon is likely related to mean water level (MWL) rise in the Gulf of Maine. Least-squares estimates of MWL trends are: 21.36 cm/century (St. John); 21.35 cm/century (Eastport); 18.82 cm/century (Portland); 28.09 cm/century (Boston). The trends of MWL in the Gulf of Maine are much bigger than those of tidal range. The Gulf of Maine is highly resonant (Garrett, 1972), but under sea level rise (SLR), the local water level is changing, and Devlin et al. (2019) have shown that this might be reducing the M_2 resonance from what has been a maximum resonance (i.e., the resonance is diminishing in intensity as water level rises), especially in the Bay of Fundy. At 1970s, the effect of SLR on the Gulf of Maine may reach the tipping point.

Why the nodal amplitudes at four stations peak in the 1985s? Previous studies (Devlin et al., 2014, 2017a; b, 2019) have indicated that tidal variability is correlated to sea level variability. However, as reported by Ray (2006), mean sea level curves for each of our four stations (Fig. A2) suggest nothing especially unusual around 1985. Since the M_2 tide is highly resonant in the Gulf of Maine, thus, it is likely sensitive to relatively small changes in the ocean. Furthermore, the ocean (such as sea surface temperature) can be easily influenced by

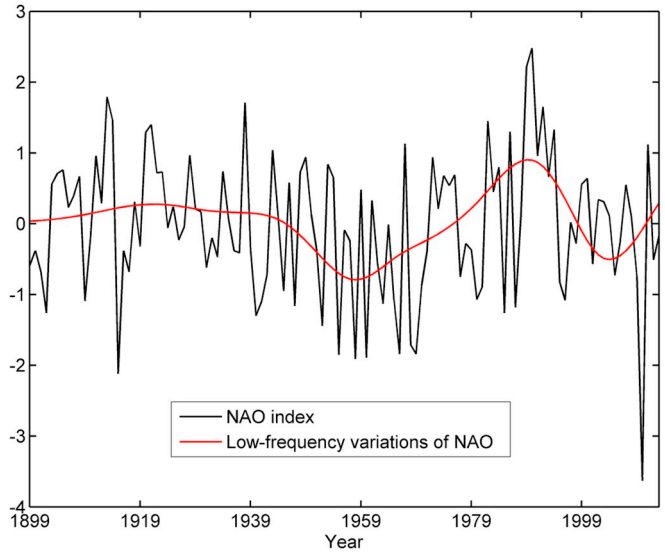

Fig. 6. The NAO index (black line) and low-frequency variations of the NAO (red line). (For interpretation of the references to colour in this figure legend, the reader is referred to the Web version of this article.)

the atmosphere. Previous study (Müller, 2011) has indicated the possible link of changing tides in the North Atlantic to the North Atlantic Oscillation (NAO) which is one of the major modes of variability of the Northern Hemisphere atmosphere (Hurrell, 1995). Therefore, we think it is possible that the NAO can also influence the nodal response of M_2 tide in the Gulf of Maine. Fig. 6 (black line) shows the annual NAO index downloaded from National Center for Atmospheric Research (NCAR). We decomposed the annual NAO index with the EMD method (Huang et al., 1998; Cheng et al., 2017; Pan et al., 2018a), obtaining 5 modes. The combination of mode 4 and mode 5 (red line in Fig. 6) reflects the low-frequency variations of the NAO. It is interesting that the low-frequency variations of the NAO are similar to the changes of nodal amplitudes from 1970 to 2013. It should be noted that the inferred correlation between the NAO and the nodal cycle may be invalid, since it is based on one low-passed fluctuation in both the nodal cycle and the NAO. The smoothing process removes degrees of freedom, thus, it is difficult to prove statistical validity. But we still believe that there is a possible connection between the NAO and the changes in the response of the nodal modulation of the M_2 tide in the Gulf of Maine. However, so far, the potential physical mechanism linking these processes remains unclear.

4. Summary and conclusion

The nodal modulation itself is not changing (i.e., the position of the sun and the moon and their associated wobbles that produce the nodal modulation are not changing). But it is true that each location on the ocean where a tide gauge is located will have a different local response to the induced nodal forcing due to the latitude, bathymetry, coastal morphology, sea level rise and changing bed friction induced by harbor modifications. Thus we see much different tides all over the world. The Gulf of Maine is a prime example of this effect and the shape of the Bay of Fundy amplifies the semidiurnal tides more than anywhere else. Therefore, we think it is perfectly reasonable to think that the response of the nodal modulation of M_2 tides in the Gulf of Maine could exhibit temporal changes. However, previous studies all assume the response of the nodal modulation is stationary, namely, the nodal amplitudes and phases are constant (Ray, 2006; Müller, 2011; Feng et al., 2015; Devlin et al., 2014, 2017a,b, 2018). This assumption works very well in most regions. However, in some special regions, this assumption may induce puzzling results, for example, the M_2 discontinuity in the Gulf of Maine in the early 1980s (Ray, 2006).

In this paper, using enhanced harmonic analysis (EHA), temporal changes in the response of the nodal modulation of the M_2 tide are extracted for the first time. The temporal variations of nodal amplitudes at four stations in the Gulf of Maine are similar from 1970s to 2013, which may be caused by the NAO. Compared to EHA, the traditional method of harmonic analysis only provides mean values of time-dependent nodal properties, but no insight into the non-stationarity caused by rising MWL and changing regional climate patterns. Furthermore, the results obtained by the new method indicate that the traditional method of harmonic analysis slightly underestimates the trend of M_2 amplitude in the Gulf of Maine.

Our method can be directly applied to other sites. But it should be noted that the optimal IP may be different as study sites are changed. The users should perform a series of sensitivity experiments, where the number of IP for the nodal cycle increases gradually from 3. As the IP number increases, both RMSE and SNR are decreasing. The optimal IP number can produce a relatively low RMSE and a relatively high SNR.

The rapidly increasing MWL and tidal ranges in the Gulf of Maine significantly increase the risk of flooding in the future. Although temporal changes in the response of the nodal modulation of the M_2 tide are not at this point well understood, our work provides a new perspective of understanding changing tides which is helpful for sea level prediction and local coastal planning. Future work will focus on uncovering the potential physical mechanism which induced temporal changes in the response of the nodal modulation.

Acknowledgements

We deeply appreciate the reviewers and editor for their constructive criticism of an early version of the manuscript. Tide data were provided by the University of Hawaii Sea Level Center (https://uhslc.soest.hawaii.edu/), and Fisheries and Oceans Canada (http://www.isdm-gdsi.gc.ca/isdm-gdsi/twl-mne/inventory-inventaire/interval-intervalle-eng.asp?user=isdm-gdsi&region=ATL&tst=1&no=65&ref=maps-cartes). The NAO index is downloaded from NCAR (https://climatedataguide.ucar.edu/climate-data/hurrell-north-atlantic-oscillation-nao-index-pc-based?qt-view_tab_summary_block_11=5#qt-view_tab_summary_block_11). The authors thank Rich Pawlowicz, Bob Beardsley, and Steve Lentz for distributing the T_TIDE package. The authors also thank G. Rilling for distributing the EMD package.

This work is supported by the National Natural Science Foundation of China through grant U1806214 and the National Key Research and Development Plan of China (Grant No. 2016YFC1402705 and 2016YFC1402304). S_TIDE toolbox can be downloaded from the website https://www.researchgate.net/project/Adaptation-of-tidal-harmonic-analysis-to-nonstationary-tides.

Appendix A

Table A1
The results of EHA at Boston (1921–2013)

IP number	Trend (cm/century)	95% confidence intervals of trend	SNR	RMSE (cm)
0	2.5544	0.6345	4.0259	0.7834
3	2.5926	0.6744	3.8441	0.7680
4	2.6014	0.6679	3.8947	0.7490
5	2.8177	0.6902	4.0823	0.7163
6	2.8527	0.7132	3.9997	0.7130
7	2.8723	0.7322	3.9231	0.6738
8	2.9075	0.7715	3.7689	0.6388
9	3.2754	1.0805	3.0313	0.6387
10	4.2441	1.8636	2.2774	0.6126
11	−0.5841	3.2853	0.1778	0.5915
12	6.6537	5.5050	1.2087	0.5729

Table A2
The results of EHA at Eastport (1929–2013)

IP number	Trend (cm/century)	95% confidence intervals of trend	SNR	RMSE (cm)
0	7.5854	1.6713	4.5387	1.805
3	7.9127	1.7376	4.5539	1.735
4	7.8599	1.8225	4.3127	1.677
5	7.8901	1.7883	4.4121	1.596
6	8.0169	1.9814	4.0461	1.596
7	7.8151	2.0911	3.7374	1.515
8	8.4317	2.8967	2.9108	1.478
9	11.3547	4.9873	2.2767	1.419
10	−0.6593	9.4746	0.0696	1.387
11	28.1325	16.5445	1.7004	1.278
12	27.9478	27.5360	1.0150	1.268

Table A3
The results of EHA at Halifax (1920–2013)

IP number	Trend (cm/century)	95% confidence intervals of trend	SNR	RMSE (cm)
0	−1.5318	0.3738	4.0983	0.4786
3	−1.7634	0.3681	4.7907	0.4375
4	−1.7478	0.3659	4.7769	0.4265
5	−1.8369	0.3780	4.8596	0.4158
6	−1.8977	0.3726	5.0937	0.3950
7	−1.9985	0.3897	5.1279	0.3846
8	−2.0342	0.4312	4.7179	0.3868
9	−1.7936	0.4725	3.7959	0.3219
10	−1.7043	0.7924	2.1509	0.3183
11	−0.7239	1.3942	0.5193	0.3113
12	−0.7870	2.4076	0.3269	0.3112

Table A4
The results of EHA at St.John (1906–2013)

IP number	Trend (cm/century)	95% confidence intervals of trend	SNR	RMSE (cm)
0	5.5398	1.8933	2.9259	2.6343
3	4.5880	1.9710	2.3277	2.4044
4	4.1991	1.8894	2.2225	2.2551
5	3.8404	1.8405	2.0865	2.0913
6	3.6501	1.8767	1.9449	2.0491
7	2.6188	1.9242	1.3610	1.8722
8	2.5151	1.9559	1.2859	1.7688
9	2.4434	2.0684	1.1813	1.6985
10	3.3144	2.3087	1.4356	1.6020
11	1.0569	2.8856	0.3663	1.6092
12	7.1089	4.5429	1.5649	1.4786

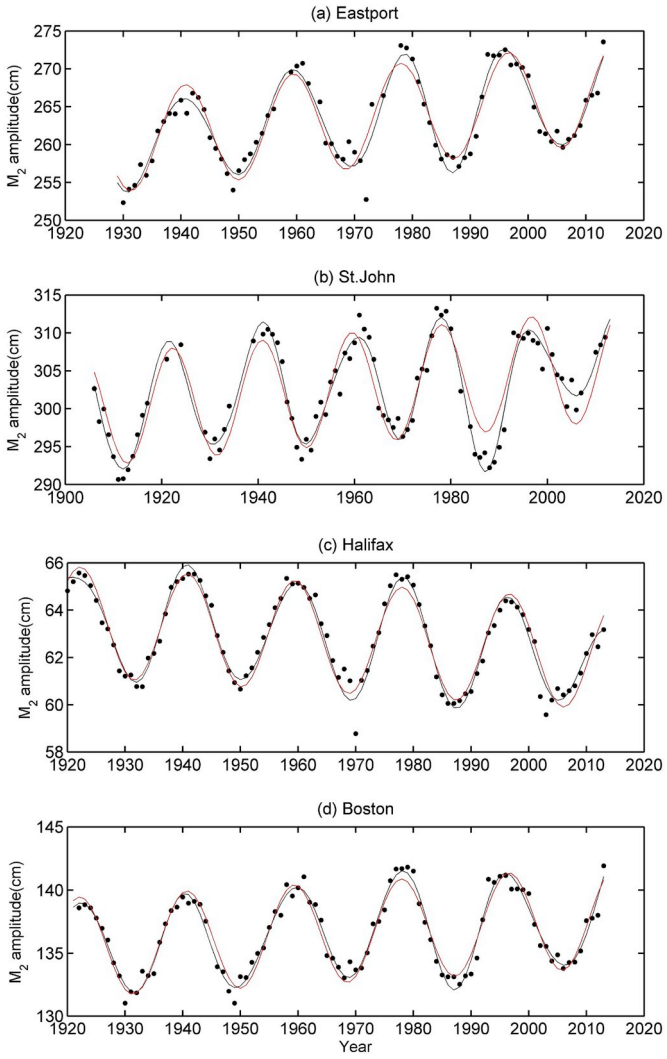

Fig. A1. Yearly estimates of the amplitude of the M_2 tide at four tide-gauge stations (black dots). The hindcasts obtained by EHA with optimal IP number (black line). The hindcasts obtained by traditional method of tidal analysis (red line).

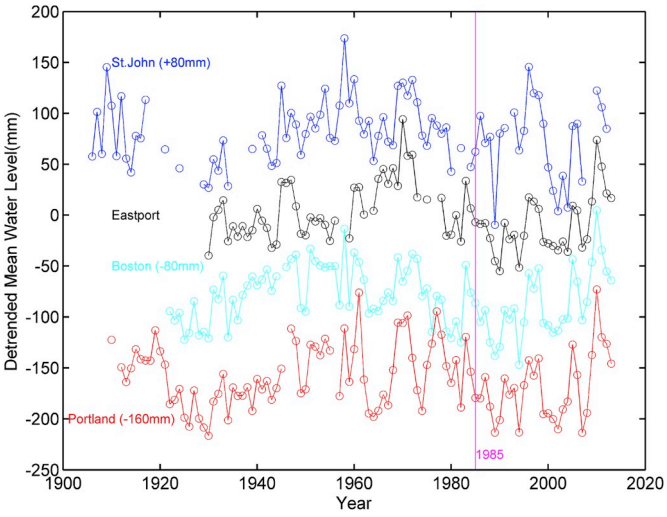

Fig. A2. Detrended mean water level variations at 4 tide-gague stations. Least-squares estimates of trends are: 21.36 cm/ century (St.John); 21.35 cm/ century (Eastport); 18.82 cm/ century (Portland); 28.09 cm/ century (Boston).2

References

Cheng, Y., Ezer, T., Atkinson, L.P., Xu, Q., 2017. Analysis of tidal amplitude changes using the EMD method. Cont. Shelf Res. 148 (September), 44–52. https://doi.org/10.1016/j.csr.2017.09.009.

Devlin, A.T., Jay, D.A., Talke, S.A., Zaron, E., 2014. Can tidal perturbations associated with sea level variations in the western Pacific Ocean be used to understand future effects of tidal evolution? Ocean Dynam. 64 (8), 1093–1120.

Devlin, A.T., Jay, D.A., Zaron, E.D., Talke, S.A., Pan, J., Lin, H., 2017a. Tidal variability related to sea level variability in the Pacific Ocean. J. Geophys. Res.: Oceans 122 (11), 8445–8463. https://doi.org/10.1002/2017JC013165.

Devlin, A.T., Jay, D.A., Talke, S.A., Zaron, E.D., Pan, J., Lin, H., 2017b. Coupling of sea level and tidal range changes, with implications for future water levels. Sci. Rep. 7 (1), 17021. https://doi.org/10.1038/s41598-017-17056-z.

Devlin, A.T., Zaron, E.D., Jay, D.A., Talke, S., 2018. Seasonality of tides in southeast asian waters. J. Phys. Oceanogr. 48 (2), 1169–1190. https://doi.org/10.1175/JPO-D-17-0119.1.

Devlin, A.T., Pan, J., Lin, H., 2019. Extended spectral analysis of tidal variability in the North Atlantic Ocean. J. Geophys. Res.: Oceans 124. https://doi.org/10.1029/2018JC014694.

Feng, X., Tsimplis, M.N., Woodworth, P.L., 2015. Nodal variations and long-term changes in the main tides on the coasts of China. J. Geophys. Res. Oceans 120, 1215–1232.

Garrett, C., 1972. Tidal resonance in the Bay of Fundy and Gulf of Maine. Nature 238, 441–443.

Godin, G., 1992. Possibility of rapid changes in the tide of the Bay of Fundy, based on a scrutiny of the records from Saint John. Cont. Shelf Res. 12, 327–338.

Godin, G., 1995. Rapid evolution of the tide in the Bay of Fundy. Cont. Shelf Res. 15, 369–372.

Greenberg, David A., Wade, Blanchard, Smith, Bruce, Barrow, Elaine, 2012. Climate change, mean sea level and high tides in the Bay of Fundy. Atmos.-Ocean 50 (3), 261–276. https://doi.org/10.1080/07055900.2012.668670.

Guo, Z., Pan, H., Fan, W., Lv, X., 2017. Application of surface spline interpolation in inversion of bottom friction Coefficients. J. Atmos. Ocean. Technol. 34 (9), 2021–2028. https://doi.org/10.1175/JTECH-D-17-0012.1.

Huang, N.E., Shen, Z., Long, S.R., Wu, M.C., Shih, H.H., Yen, N., Tung, C.C., Liu, H.H., 1998. The Empirical Mode Decomposition and the Hilbert Spectrum for Nonlinear and Non-stationary Time Series Analysis. vol. 454. R. Soc. Publ., pp. 903–995. https://doi.org/10.1098/rspa.1998.0193. 1971.

Hurrell, J.W., 1995. Decadal trends in the North Atlantic Oscillation and relationships to regional temperature and precipitation. Science 269, 676–679.

Jay, D.A., 2009. Evolution of tidal amplitudes in the eastern Pacific Ocean. Geophys. Res. Lett. 36, L04603.

Jin, G., Pan, H., Zhang, Q., Lv, X., Zhao, W., Gao, Y., 2018. Determination of harmonic parameters with temporal variations: An enhanced harmonic analysis algorithm and application to internal tidal Currents in the South China sea. J. Atmos. Ocean. Technol. 35 (7), 1375–1398. https://doi.org/10.1175/JTECH-D-16-0239.1.

Katavouta, A., Thompson, K.R., Lu, Y., Loder, J.W., 2016. Interaction between the tidal and seasonal variability of the Gulf of Maine and Scotian Shelf region. J. Phys. Oceanogr. 46 (11), 3279–3298.

Ku, L.-F., Greenberg, D.A., Garrett, C.J.R., Dobson, F.W., 1985. Nodal modulation of the lunar semidiurnal tide in the Bay of Fundy and Gulf of Maine. Science 230, 69–71.

Lu, X., Zhang, J., 2006. Numerical study on spatially varying bottom friction coefficient of a 2D tidal model with adjoint method. Cont. Shelf Res. 26 (16), 1905–1923. https://doi.org/10.1016/j.csr.2006.06.007.

Müller, M., 2011. Rapid change in semi-diurnal tides in the North Atlantic since 1980. Geophys. Res. Lett. 38, L11602.

Pan, H., Guo, Z., Lv, X., 2017. Inversion of tidal open boundary Conditions of the M2 constituent in the bohai and yellow seas. J. Atmos. Ocean. Technol. 34 (8), 1661–1672. https://doi.org/10.1175/JTECH-D-16-0238.1.

Pan, H., Guo, Z., Wang, Y., Lv, X., 2018a. Application of the EMD method to river tides. J. Atmos. Ocean. Technol. 35 (4), 809–819. https://doi.org/10.1175/JTECH-D-17-0185.1.

Pan, H., Lv, X., Wang, Y., Matte, P., Chen, H., Jin, G., 2018b. Exploration of tidal-fluvial interaction in the Columbia River estuary using S_TIDE. J. Geophys. Res. Ocean. 123 (9), 6598–6619. https://doi.org/10.1029/2018JC014146.

Pan, H., Lv, X., 2019. Reconstruction of spatially continuous water levels in the Columbia River Estuary : The method of empirical orthogonal function revisited. Estuar. Coast Shelf Sci. 222 (April), 81–90. https://doi.org/10.1016/j.ecss.2019.04.011.

Pawlowicz, R., Beardsley, B., Lentz, S., 2002. Classical tidal harmonic analysis including error estimates in MATLAB using T_TIDE. Comput. Geosci. 28 (8), 929–937. https://doi.org/10.1016/S0098-3004(02)00013-4.

Pelling, H.E., Green, J.A.M., 2013. Sea level rise and tidal power plants in the Gulf of Maine. J. Geophys. Res. Oceans 118, 2863–2873. https://doi.org/10.1002/jgrc.20221.

Ray, R.D., 2006. Secular changes of the M2 tide in the Gulf of Maine. Cont. Shelf Res. 26, 422–427.

Ray, R.D., 2009. Secular changes in the solar semidiurnal tide of the western North Atlantic Ocean. Geophys. Res. Lett. 36, L19601.

Ray, R.D., Foster, G., 2016. Future nuisance flooding at Boston caused by astronomical tides alone. Earth's Future 4, 578–587. https://doi.org/10.1002/2016EF000423.

Wang, Z.A., Lawson, G.L., Pilskaln, C.H., Maas, A.E., 2017. Seasonal controls of aragonite saturation states in the Gulf of Maine. J. Geophys. Res. Oceans 122, 372–389. https://doi.org/10.1002/2016JC012373.

Zong, X., Pan, H., Liu, Y., Lv, X., 2018. Improved estimation of pollutant emission rate in an ocean pollutant diffusion model by the application of spline interpolation with the adjoint method. J. Atmos. Ocean. Technol. 35 (10), 1961–1975. https://doi.org/10.1175/JTECH-D-17-0208.1.